Power law persistence in the atmosphere and in the oceans

Armin Bunde[a] and Shlomo Havlin[b]

[a] *Institut für Theoretische Physik III, Universität Giessen, D-35392 Giessen, Germany*

[b] *Minerva Center and Department of Physics, Bar Ilan University, Israel*

In honor of our dear friend H. Eugene Stanley for his 60^{th} birthday

Abstract

The persistence of the weather is a well known phenomenon. If, for example, one day is sunny and warm, there is a high tendency that the next day remains similar. In this paper, we review recent results showing that the long term persistence, characterized by the correlation $C(s)$ of temperature variations separated by s days, decays for large s as a power law. For continental stations, the exponent is always close to 0.7, while for stations on islands as well as for sea surface temperatures, the exponent is close to 0.4. In contrast to the temperature fluctuations, the fluctuations of the rainfall usually are not characterized by long term power law correlations but rather by short term correlations. The universal persistence law for the temperature fluctuations on continental stations represents an ideal (and uncomfortable) test bed for the state-of-the-art global climate models and allows to evaluate their performance.

1. Introduction

Characterizing the complex variabilty at all temporal and spatial scales remains one of the most important challenges of research [1–6]. In recent years, considerable amount of effort has been devoted to analyzing temporal correlations that characterize the persistence of weather and climate regimes. The short term persistence of weather states is a well-known phenomenon: there is a strong tendency for subsequent days to remain similar, a warm day is more likely to be followed by a warm day than by a cold day and vice versa. The typical time scale for weather changes is about one week, a time period which corresponds to the average duration of so-called "general weather regimes" or "Grosswetterlagen". This property of persistence is often used as a "minimum skill" forecast for assessing the usefulness of short to medium range numerical weather forecasts. Longer term persistence of synoptic regimes up to time scales of several weeks is often related to circulation patterns

associated with blocking [7]. A blocking situation occurs when a very stable high pressure system is established over a particular region and remains in place for several weeks, as opposed to the usual time scale of 3-5 days for synoptic systems. As a result the weather in the region of the high remains fairly persistent throughout the period. Furthermore, transient low pressure systems are deflected around the blocking high so that the region downstream of the high experiences a larger than usual number of storms.

There have been also indications that weather persistence exists over many months or seasons [8], between successive years, and even over several decades [9,10]. Such persistence is usually associated with slowly varying external (boundary) forcing such as sea surface temperatures and anomaly patterns. On the scale of months to seasons, one of the most pronounced phenomenon is the El Nino Southern Oscillation (ENSO) event which occurs every 3-5 years and which strongly affects the weather over the tropical Pacific as well as over North America [11]. On the even longer multidecadal to century time scales, external forcing associated with anthropogenic effects (e.g. increasing greenhouse gases and changing land use) also appear to play an important role in addition to the natural variability of the climate system [12].

To avoid detection of spurious correlations arising from nonstationarities, new statistical-physics tools such as wavelet techniques (WT) (see e. g. [13]) and detrended fluctuation analysis (DFA) (see, e. g. [14–17]) have been developed recently. DFA and WT can systematically eliminate trends in the data and thus reveal intrinsic dynamical properties such as distributions, scaling and long-range correlations very often masked by nonstationarities. In recent studies [18–20] we have applied DFA and WT to study temperature and precipitation correlations in different climatic zones on the globe, as well as correlations in the sea surface temperature of the oceans.

The results indicate that both the athmospheric temperature and the sea temperatures are long range power law correlated. Their long term persistence, characterized by the auto-correlation $C(s)$ of temperature variations separated by s days, decays as

$$C(s) \sim s^{-\gamma}. \tag{1}$$

The exponent γ has roughly the same value $\gamma \cong 0.7$ for all continental records. The sea surface temperature as well as the athmospheric temperatures of small islands exhibit stronger long term correlations, with smaller values of γ. In contrast, for most stations the precipitation records do not show indications of long term correlations on scales above 6 months. The fact that the correlation exponent varies only very little for the continental athmospheric temperatures, presents an ideal test bed for the performance of the global climate models [21].

The paper is organized as follows: In Section 2, we describe the detrending analysis methods. Then, in Section 3, we review the application of these methods to both atmospheric and sea surface temperature. In Section 4, we describe the studies on the precipitation fluctuations, and finally, in Section 5, we describe how the "universal" persistence law for the atmospheric temperature fluctuations on continental stations can be used to test the climate models.

2. The methods of analysis

Consider, e.g., a record T_i, where the index i counts the days in the record, $i = 1,2,...,N$. The T_i may represent mean daily temperatures (of air or water) or daily amount of precipitation measured at a certain meteorological station. For eliminating the periodic seasonal trends, we concentrate on the departures of the T_i, $\Delta T_i = T_i - \overline{T}_i$, from their mean daily value $\overline{T}_i$ for each calendar date i, say 1^{st} of April, which has been obtained by averaging over all years in the record.

Quantitatively, correlations between ΔT_i separated by n days are defined by the (auto) correlation function,

$$C(n) \equiv \langle \Delta T_i \Delta T_{i+n} \rangle = \frac{1}{N-n} \sum_{i=1}^{N-n} \Delta T_i \Delta T_{i+n}. \tag{2}$$

If the ΔT_i are uncorrelated, $C(n)$ is zero for n positive. If correlations exist up to a certain number of days $n_\times$, the correlation function will be positive up to $n_\times$ and vanish above $n_\times$. A direct calculation of $C(n)$ is hindered by the level of noise present in the finite records, and by possible nonstationarities in the data. To reduce the noise we do not calculate $C(n)$ directly, but instead study the "profile"

$$Y_m = \sum_{i=1}^{m} \Delta T_i. \tag{3}$$

We can consider the profile Y_m as the position of a random walker on a linear chain after m steps. The random walker starts at the origin and performs, in the ith step, a jump of length ΔT_i to the right, if ΔT_i is positive, and to the left, if ΔT_i is negative. According to random walk theory, the fluctuations $F^2(s)$ of the profile, in a given time window of size s, are related to the correlation function $C(s)$. For the relevant case (1) of long-range power-law correlations, $C(s) \sim s^{-\gamma}$, $0 < \gamma < 1$, the mean-square fluctuations $\overline{F^2(s)}$, obtained by averaging over many time windows of size s (see below) increase by a power law [22],

$$\overline{F^2(s)} \sim s^{2\alpha}, \quad \alpha = 1 - \gamma/2. \tag{3}$$

For uncorrelated data (as well as for correlations decaying faster than $1/s$), we have $\alpha = 1/2$.

For the analysis it is useful to employ a hierarchy of methods that differ in the way the fluctuations are measured and possible trends are eliminated (for a detailed description of the methods we refer to [17]).

(i) In the simplest type of fluctuation analysis (FA) (where trends are not eliminated), we determine the difference of the profile at both ends of each segment. The square of this difference represents the square of the fluctuations in each segment.

(ii) In the *first order* detrended fluctuation analysis (DFA1), we determine in each segment the best linear fit of the profile. The variance of the profile from this straight line represents the square of the fluctuations in each segment.

(iii) In general, in the n-th order DFA (DFAn) we determine in each segment the best n-th order polynomial fit of the profile. The variance of the profile from these best n-th order polynomials represents the square of the fluctuations in each segment.

By definition, FA does not eliminate trends and it is thus similar to the Hurst method and the conventional power spectral method [23]. In contrast, DFAn eliminates trends of order n in the profile and $n-1$ in the original time series. Thus, from the comparison of fluctuation functions $F(s)$ obtained from different methods one can learn about long term correlations and types of trends, which cannot be achieved by the conventional techniques.

3. Analysis of temperature records

3.1. Atmospheric temperatures

Figure 1 shows the results of the FA and DFA analysis of the mean daily temperatures T_i of the following weather stations (length of record is in parentheses): Cheyenne (USA, 123 y) and Kasan (Russia, 111 y) (Fig. 1a,b), Sydney (108 y) and Plymouth (122 y) (Fig. 1c,d), and Cocos Island (Australia, 46y) and Wuxqiaoling Summit (China, 40y) (Fig. 1e,f). The results are typical for a large number of records that we have analyzed so far (see [18,24]). Cheyenne and Kasan have continental climate, Sydney and Plymouth are on coastlines, Cocos Island is a small island in the Pacific ocean, and the weather station of Wuxqiaoling is on top of a mountain.

In the log-log plots, all curves are (except at small s-values) approximately straight lines. For both stations inside the continents and along coast lines the slope is $\alpha \cong 0.65$. There exists a natural crossover (above the DFA-crossover) that can be best estimated from FA and DFA1. As can be verified easily, the crossover occurs roughly at $t_c = 10d$, which is the order of magnitude for a typical Grosswetterlage. Above t_c, there exists long-range persistence expressed by the power-law decay of the correlation function with an exponent $\gamma = 2 - 2\alpha \cong 0.7$. The results indicate that the exponent is "universal" , i.e. does not depend on the location or the climatic zone of the weather station. Below t_c, the fluctuation functions do not show universal behavior and reflect the different climatic zones.

However, there are exceptions from this universal behavior, and these occur for locations on small islands and on top of large mountains. In the first case, the exponent can be considerably larger, typically $\alpha \cong 0.8$, corresponding to $\gamma \cong 0.4$. In the second case, on top of a mountain, the exponent can be considerably smaller, usually $\alpha \cong 0.58$, corresponding to $\gamma \cong 0.84$.

3.2. Sea surface temperatures (SST)

Next we consider the persistence in the sea surface temperature studied for different sites in the Atlantic and Pacific oceans. Monetti *et al.* [20] applied the FA and DFA methods

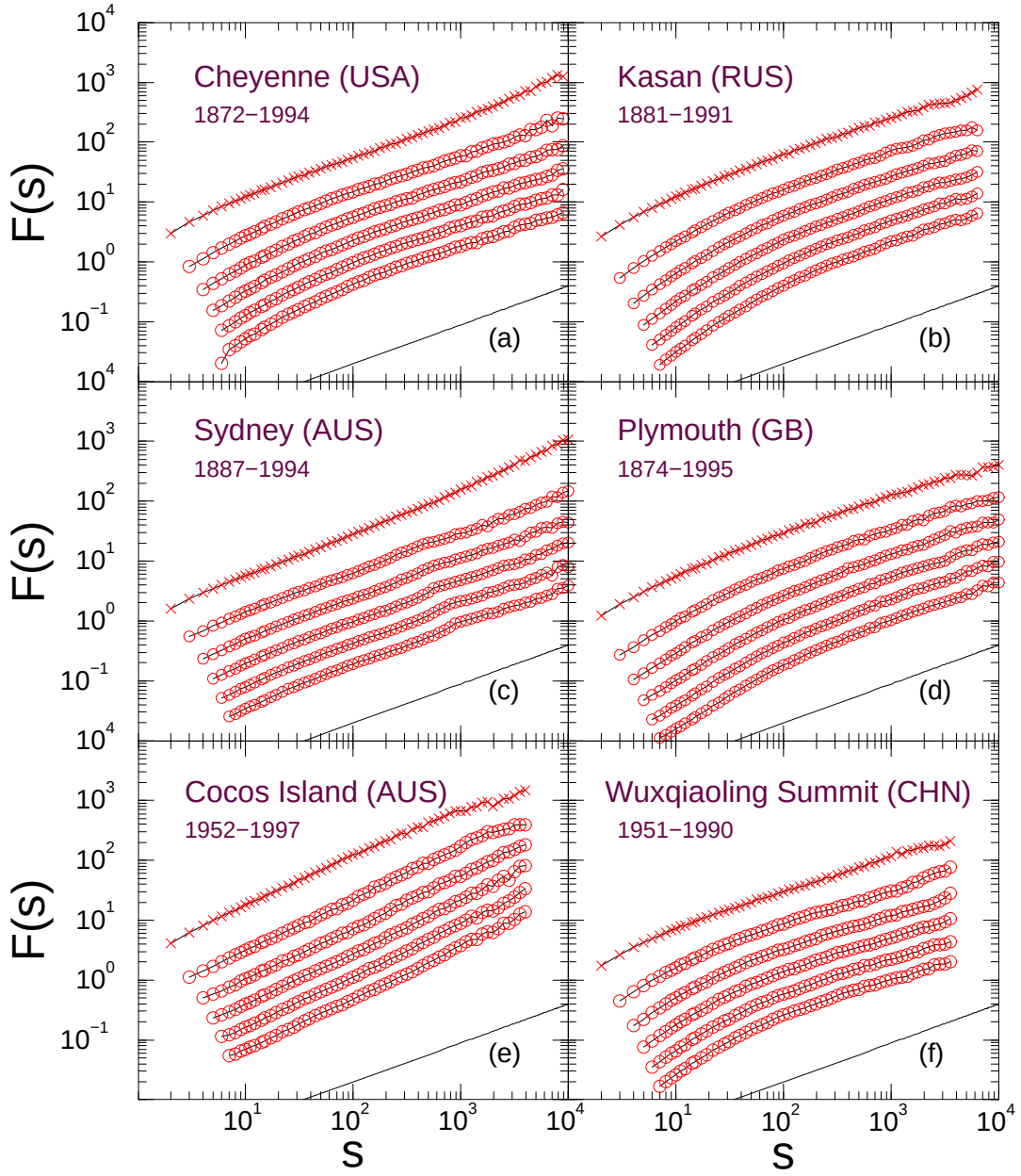

Fig. 1. Analysis of mean daily temperature records of 6 representative weather stations. The 6 figures show the fluctuation functions obtained by FA, DFA1, DFA2, DFA3, DFA4, and DFA5 (from top to bottom) for the 6 sets of data. The scale of the fluctuation functions is arbitrary. A line with slopes 0.65 is shown as guide to the eye. After [24].

to 36 (46) monthly SST records and 64 (35) weekly SST records in the Atlantic (Pacific) ocean to characterize the persistence in the SST. Figure 2 (a) shows that $t > t_c$ Prague temperature fluctuations display a power law behavior. The fluctuation exponent obtained from the FA ($\alpha \cong 0.81$) is greater than the values given by the DFA1-5 ($\alpha \cong 0.65$). This difference can be attributed to the well known effect of urban warming of Prague. The fluctuation exponent $\alpha \approx 0.65$ is consistent with the earlier finding, where the whole Prague record (218 years) has been analyzed [18]. Figure 2(a) shows that the FA (and the similar Hurst and power spectrum methods) may lead to spurious results because of the presence of trends, yielding a large overestimation of long range correlations.

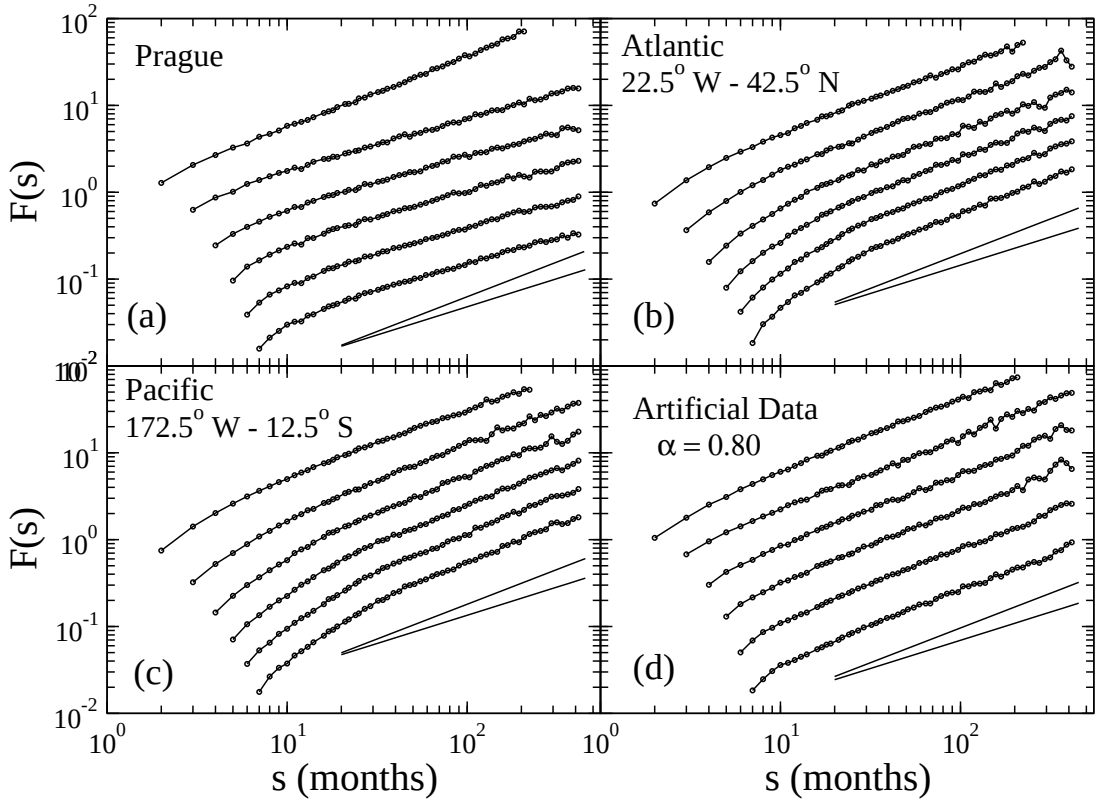

Fig. 2. Log-log plots of the FA and the DFA for Prague, Atlantic ocean, Pacific ocean and artificial data. ¿From top to bottom curves correspond to FA, DFA1 to DFA5. Lines of slope 0.8 and 0.65 have drawn to compare the typical SST asymptotic fluctuation exponent with the atmospheric land temperature fluctuation exponent. After [20].

Figures 2(b) and 2(c) show the FA and DFA results for two typical sites in the Atlantic and Pacific oceans, respectively. Here, at long time scales, FA and DFA curves are straight lines with roughly the same fluctuation exponent $\alpha \sim 0.8$. This shows that (a) trends do not falsify the FA result and therefore may be regarded as much less important than for Prague temperatures, and (b) long range correlations also occur in SST's. These correlations are stronger than the correlations in the atmospheric land temperatures, since the fluctuation exponent $\alpha \sim 0.8$ corresponds to a correlation exponent $\gamma \sim 0.4$. As in the case of atmospheric land temperatures, the range of this persistence law seems to exceed one decade and is possible even longer than the range of the SST series considered.

In contrast to Prague, there is a pronounced short-time regime which ends roughly at 10 months. This regime can be better revealed by the analysis of the weekly SST series [20]. The short time SST exhibits a persistence which is considerably stronger than the SST long term persistence and the atmospheric land temperature persistence. The typical SST short-time fluctuation exponent is $\alpha \approx 1.20$. However, in the northern Atlantic (latitudes from 30^o to 50^o north) even higher fluctuation exponents are found ($\alpha \cong 1.4$). As seen from Fig. 2(d) for artificial data DFA yeild the same fluctation exponent for both short term and long term. Thus the crossover in Figs. 2 (b) and 2 (c) is due to intrinsic correlations and not artifact of DFA. Since the exponent in continental and coastline stations does not depend on the location of the meteorological station and its local environment, the power law behavior can serve as an ideal test for climate models where regional details

cannot be incorporated and therefore regional phenomena like urban warming cannot be accounted for. The power law behavior seems to be a global phenomenon and therefore should also show up in the simulated data of the global climate models (GCM).

Next we consider precipitation records.

4. Analysis of precipitation records

Figure 3 shows the results of the FA and DFA analysis of the daily precipitation T_i of the following weather stations (length of record is in parentheses): Cheyenne (USA, 117 y) and Kasan (Russia, 119 y) (Fig. 1a,b), Sydney (113 y) and Plymouth (124 y) (Fig. 1c,d), and Norfolk Island (Australia, 59y) and Wuxqiaoling Summit (China, 40y) (Fig. 1e,f). The stations are, except for the island, the same as in Fig. 1. The results are typical for a large number of records that we have analyzed so far (see [19]).

In the log-log plots, all curves are (except at small s-values) approximately straight lines at large times, with a slope close to 0.5. If there exist long range correlations, then they are very weak. Some exception are stations on top of a mountain, where the exponent might be around 0.6, but this happens only very rarely. In most cases, the exponent is between 0.5 and 0.55, pointing to uncorrelated or weakly correlated behavior at large time spans. Unlike to the temperature records, the exponents actually do not depend on specific climatic or geographic conditions.

5. Test of global climate models

The state-of-the-art global climate models (GCMs) provide numerical solutions of the Navier Stokes equations devised for simulating meso-scale to large-scale atmospheric and oceanic dynamics. In addition to the explicitly resolved scales of motions, the models also contain parameterization schemes representing the so-called subgrid-scale processes, such as radiative transfer, turbulent mixing, boundary layer processes, cumulus convection, precipitation, and gravity wave drag. A radiative transfer scheme, for example, is necessary for simulating the role of various greenhouse gases such as CO_2 and the effect of aerosol particles. The differences among the models usually lie in the selection of the numerical methods employed, the choice of the spatial resolution [25], and the detailed formulation of the subgrid-scale parameterization schemes.

These scenarios have been studied by the models, and the results are available from the IPCC Data Distribution Center [26]. The first scenario is control run with fixed CO_2 content. In the second scenario, one considers only the effect of greenhouse gas forcing. The amount of greenhouse gases is taken from the observations until 1990 and then increased at a rate of 1% per year. In the third scenario, also the effect of aerosols (mainly sulphates) in the atmosphere is taken into account which can mitigate and partially offset the greenhouse gas warming.

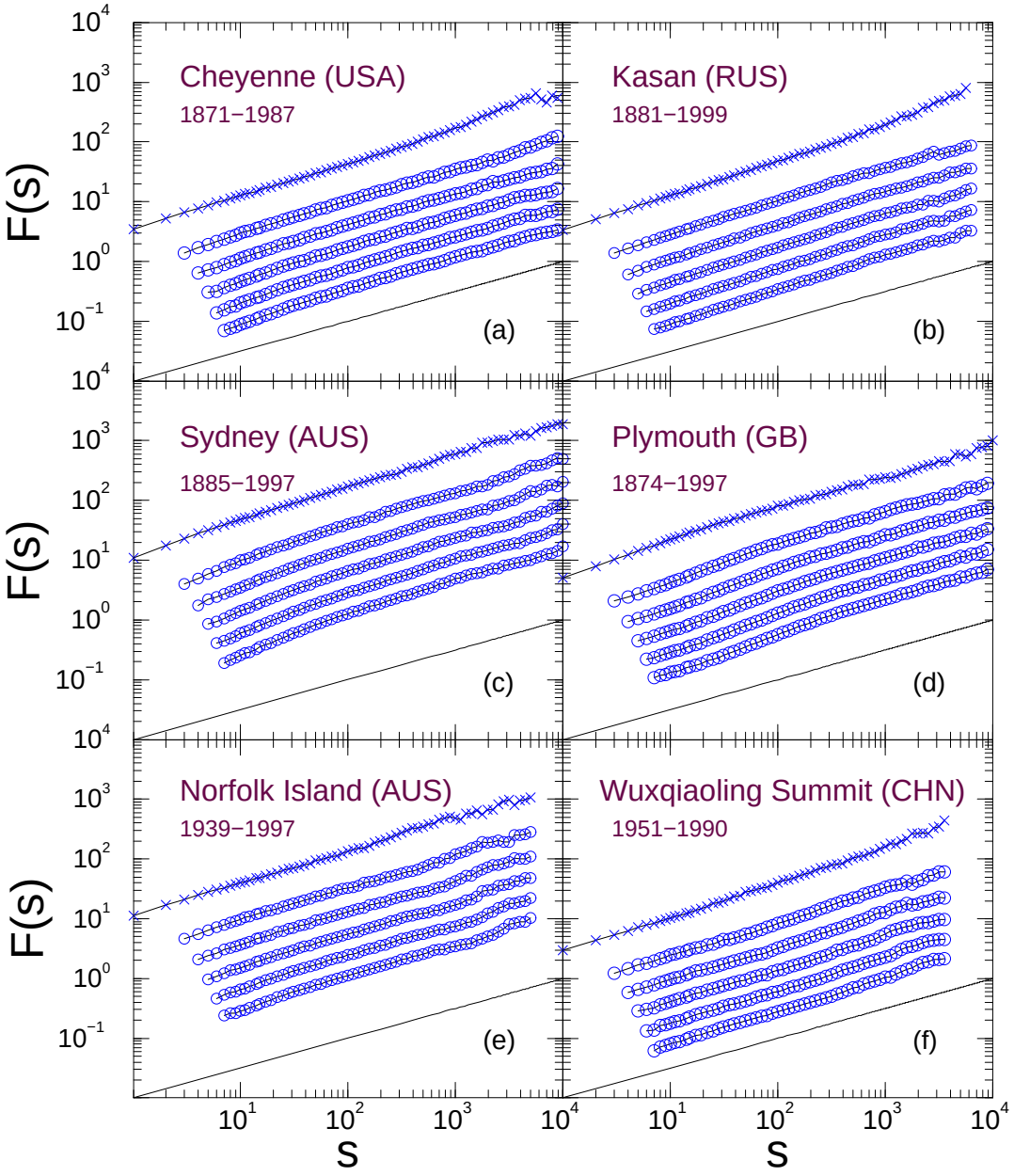

Fig. 3. Analysis of daily precipitation records of 6 representative weather stations. The 6 figures show the fluctuation functions obtained by FA, DFA1, DFA2, DFA3, DFA4, and DFA5 (from top to bottom) for the 6 sets of data. The scale of the fluctuation functions is arbitrary. A line with slopes 0.5 is shown as guide to the eye. After [19].

This third scenario, however, has to be considered as rather preliminary since the concentration and distributions of aerosols are uncertain and the precise role of aerosoles in the process of global warming is not yet fully understood.

For the test, Govindan *et al.* considered the monthly temperature records from seven GCMs: GFDL-R15-a (Princeton), CSIRO-Mk2 (Melbourne), ECHAM4/OPYC3 (Hamburg), HADCM3 (Bracknell, UK), CGCM1 (Victoria, Canada), CCSR/NIES (Tokyo),

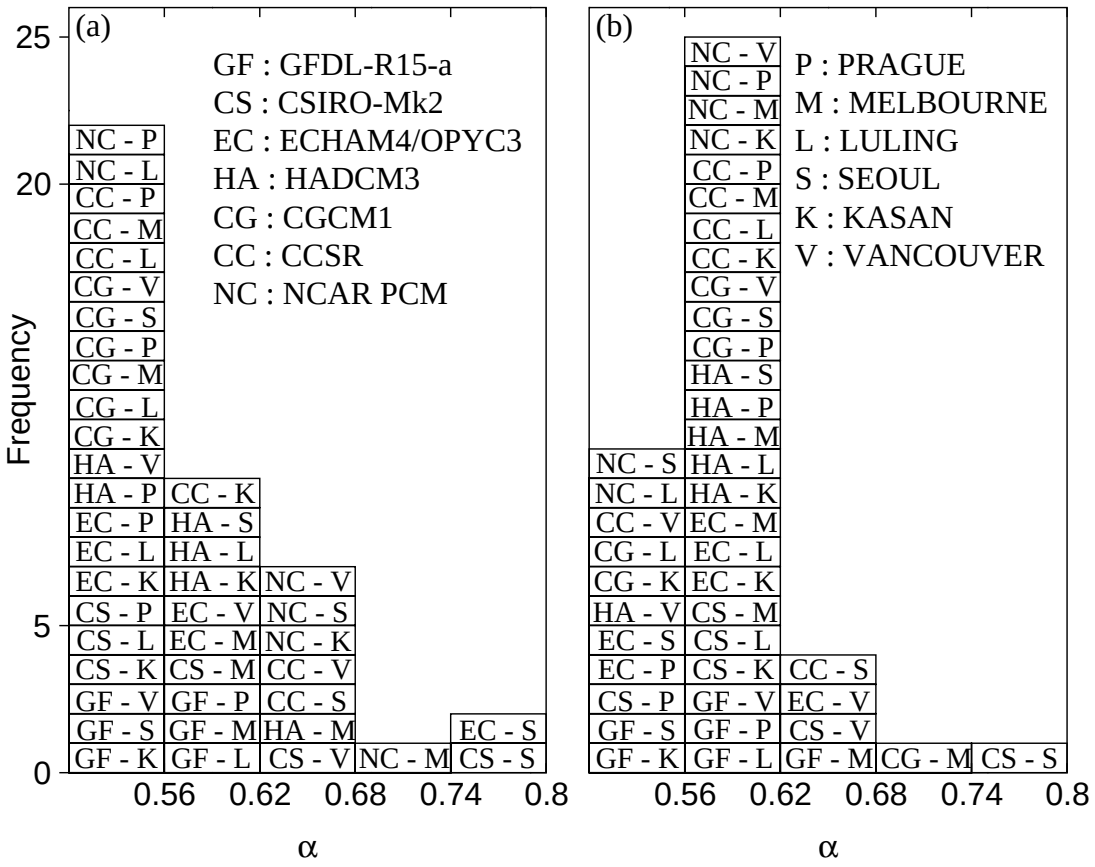

Fig. 4. Histogram of the fluctuation exponent (α) values obtained for the six sites simulated by the seven AOGCMs (a) scenario (i) and (b) scenario (ii) for the entire records. The entries in each box represent 'Model - Site'. After [21].

NCAR PCM (Boulder, USA) (see [25] for details). The data was extracted for six representative sites around the globe (Prague, Kasan, Seoul, Luling/Texas, Vancouver, and Melbourne). For each model and each scenario, the temperature records of the 4 grid points closest to each site were selected, and bilinearly interpolated the data to the location of the site. Both scenarios have been analyzed but with more focus on the better established first scenario.

The actual long term exponents α for the greenhouse gas only scenario obtained by the seven models for the six sites are summarized in a histogram in Fig. 4a. The histogram shows a pronounced maximum at $\alpha = 0.5$. For best performance, all models should have exponents α close to 0.65, corresponding to a peak of height 42 in the window. Actually more than half of the exponents are close to 0.5, while only 7 exponents are in the proper window between 0.62 and 0.68.

Figure 4b shows the histogram for scenario (ii), where in addition to the greenhouse gas forcing, also the effects of aerosols are taken into account. For this case, there is a pronounced maximum in the α window between 0.56 and 0.62 (more than half of the exponents are in this window), while only 4 exponents are in the proper range between 0.62 and 0.68. This shows that although the second scenario is also far from reproducing the scaling behavior of the real data, its overall performance is better than the performance of the first scenario.

Acknowledgement: we wish to thank the Deutsche Forschungsgemeinschaft and the Israel Science Foundation for financial support.

References

[1] IPCC: *The Regional Impacts of Climate Change*. An Assessment of Vulnerability. (University Press, Cambridge, 1998).

[2] P.M. Blaikie, T. Cannon, I. Davi and B. Wisner: *At Risk: Natural Hazards, Vulnerability and Disaster*s. (Routledge, London, 1994).

[3] H. Grassl: Global climate change, Interdisciplinary Science Reviews 24, (3) 185-194, (1999).

[4] H.J. Schellnhuber: NATURE 402, (6761) C19-C23 Suppl., (1999).

[5] K. Hasselmann: Climate Dynamics 13, 601 (1997) and the references in there.

[6] WCRP: *Climate Variability & Predictability, CLIVAR Initial Implementation Plan*, WCRP No. 103 (1998).

[7] J.G. Charney and J.G. Devore: J. Atmos. Sci. 36, 1205 (1979).

[8] J. Shukla: Science 282, 728-731 (1998).

[9] R.L. Molinari, D.A. Mayer, J.F. Festa, and H.F. Bezdek: The Journal Geophysical Research 102, 3267 (1997).

[10] R.T. Sutton and M.R. Allen: Nature 388, 563 (1997).

[11] S.G. Philander: *El Nino, La Nina and the Southern Oscillation*. International Geophysics Series, Vol 46 (1990).

[12] K. Hasselmann: Science 276, 914-915 (1997).

[13] A. Arneodo, E. Bacry, P. V. Graves, and J. F. Muzy: Phys. Rev. Lett. 74, 3293 (1995); A. Arneodo et al: Physica D 96, 291 (1996).

[14] P.Ch. Ivanov, A. Bunde, L.A.N. Amaral, S. Havlin, J. Fritsch-Yelle, R.M. Baevsky, H.E. Stanley, A.L. Goldberger: Europhys. Lett., 48, 59, 4 (1999).

[15] A. Bunde, S. Havlin, J.W. Kantelhardt, T. Penzel, J.H. Peter, K. Voigt: Phys. Rev. Lett. (2000).

[16] C.-K. Peng S.V. Buldyrev, A.L. Goldberger, S. Havlin, F. Sciortino, M. Simons, H.E. Stanley: Nature 356, 168 (1992); S. V. Buldyrev, A.L. Goldberger, S. Havlin, C.K. Peng, M. Simons, F. Sciortino: Phys. Rev. Lett. 71, 1776 (1993);S.V. Buldyrev, A.L. Goldberger, S. Havlin, R.N. Mantegna, M.E. Matsa ME, C.-K. Peng, M. Simons, H.E. Stanley: Phys. Rev. E 51, 5084 (1995).

[17] J. W. Kantelhardt, E. Koscielny-Bunde, H. A. Rego, S. Havlin, A. Bunde, Detecting long-range correlations with detrended fluctuation analysis, Physica A **295**, 441 (2001).

[18] E. Koscielny-Bunde, A. Bunde, S. Havlin, H. E. Roman, Y. Goldreich, H.-J. Schellnhuber: Phys. Rev. Lett. 81, 729 (1998); E. Koscielny-Bunde, H.E. Roman, A. Bunde, S. Havlin, H.J. Schellnhuber: Phil. Mag. B 77, 1331 (1998); E. Koscielny-Bunde, A. Bunde, S. Havlin, Y. Goldreich: Physica A 231, 393 (1996)

[19] Rybski et al, paper on Precipitaion, preprint.

[20] R. A. Monetti, S. Havlin and A. Bunde, preprint (2002).

[21] R. B. Govindan, D. Vjushin, S. Brenner, A. Bunde, S. Havlin, H.-J. Schellnhuber, Long-range correlations and trends in global climate models: Comparison with real data, Physica A 294, 239 (2001).

[22] A. Bunde and S. Havlin (eds.): *Fractals in Science*, Springer, New York (1995).

[23] J. Feder: Fractals, Plenum, New York (1989).

[24] Eichner et al, preprint.

[25] A typical climate module within the overall AOGCM machinery will have a grid spacing of 300-500 km and 10-20 vertical layers as compared to a weather forecasting model with a grid spacing of 100 km or less and 30-40 layers.

[26] http://ipcc-ddc.cru.uea.ac.uk/dkrz/dkrz_index.html